JOURNAL OF SPACECRAFT AND ROCKETS
Vol. 31, No. 2, March–April 1994

Applications of Computational Fluid Dynamics to the Aerodynamics of Army Projectiles

Walter B. Sturek,* Charles J. Nietubicz,† Jubaraj Sahu‡, and Paul Weinacht§
U.S. Army Research Laboratory, Aberdeen Proving Ground, Maryland 21005

The ability to predict the complete set of aerodynamic performance parameters for projectile configurations is the goal of the computational aerodynamicists at the U.S. Army Research Laboratory. To achieve this goal, predictive capabilities that use Navier-Stokes computational techniques have been developed and applied to an extensive number of projectile configurations. A summary of code validation efforts and applications for both spin-stabilized and fin-stabilized projectile configurations are described. Significant progress in the predictive capability for projectile aerodynamics has been achieved through the availability of substantial supercomputer resources and modern computational techniques. Current and future research areas of interest are described and provide an indication of computer resources and code enhancements needed to continue the progress in projectile computational aerodynamics.

Nomenclature

A	=reference area, $\pi D^2/4$, m^2
a	=speed of sound, m/s
C_{D_0}	=zero yaw drag coefficient
CG	=center of gravity, L/D
C_{l_0}	=roll-producing moment coefficient
C_{l_p}	=roll-damping coefficient
C_m	=pitching moment coefficient
C_{m_α}	=slope of normal force coefficient evaluated at $\alpha=0$, $dC_m/d\alpha$
$C_{m_q}+C_{m_{\dot\alpha}}$	=pitch-damping moment coefficient
C_N	=normal force coefficient
C_{N_α}	=slope of normal force coefficient
C_p	=pressure coefficient, $(p-p\infty)/(1/2\,\rho_\infty u_\infty^2)$
C_Y	=Magnus (side) force coefficient
D	=reference diameter of model, m
d	=local diameter of model, m
I	=mass injection parameter, $\dot m(\rho_\infty u_\infty A_b)$
L	=length, m
M	=Mach number
$\dot m$	=mass flow rate of injected gas $\rho_j u_j A_j$
P	=pressure normalized by $\rho_\infty a_\infty^2$ (also spin rate, rad/s)
PD/V	=nondimensional spin rate
Re	=Reynolds number
T	=temperature, K
u	=velocity component in the x direction, m/s
V	=freestream velocity, m/s
v	=velocity component in the y direction, m/s
x, y, z	=Cartesian coordinates
α	=angle of attack, deg
ρ	=density, normalized by ρ_∞
ω	=axial spin rate, rad/s

Subscripts

b	=base
j	=jet or bleed conditions
w	=body surface values
$oinj$	=injected gas
∞	=freestream conditions

Received Oct. 9, 1992; revision received Jan. 4, 1993; accepted for publication Jan. 4, 1993. This paper is declared a work of the U.S. Government and is not subject to copyright protection in the United States.

*Chief, Computational Science and Technology Division, Advanced Computational and Information Sciences Directorate, AMSRL-CI-C. Associate Fellow AIAA.

†Deputy Chief, Aerodynamics Branch, Propulsion and Flight Division, Weapons Technology Directorate, AMSRL-WT-PB. Associate Fellow AIAA.

‡Aerospace Engineer, Aerodynamics Branch, Propulsion and Flight Division, Weapons Technology Directorate, AMSRL-WT-PB. Associate Fellow AIAA.

§Aerospace Engineer, Aerodynamics Branch, Propulsion and Flight Division, Weapons Technology Directorate, AMSRL-WT-PB. Senior Member AIAA.

I. Introduction

THE objectives of this article are to provide a summary of recent computational aerodynamic efforts at the U.S. Army Ballistic Research Laboratory (BRL), now reorganized as part of the newly formed U.S. Army Research Laboratory (ARL); to provide an assessment of the current computational fluid dynamics (CFD) capabilities as applied to Army shell; and to indicate high-priority research areas for further development of the predictive technology.

This report is the third summary discussion of CFD code validation and application to projectile aerodynamics. The first paper[1] reported the status of initial efforts to apply time-marching and space-marching techniques to bodies of revolution at transonic and

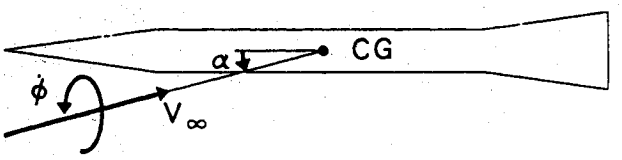

Fig. 1 Schematic of coning motion.

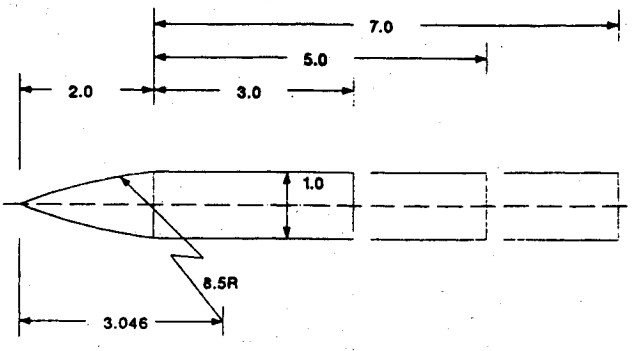

Fig. 2 Geometry of Army-Navy spinner rocket.

supersonic velocities during the period 1978–83. The second paper[2] reported similar efforts during the period 1983–88 and also included some initial results for modeling of fin-stabilized shells. The results emphasized here are relatively recent. They consist of examples of code validation, where the computational results were compared with established experimental data, and application, where the codes were used to predict the performance of proposed projectile designs.

II. Codes

The computational codes employed at the ARL for projectile aerodynamics emphasize Reynolds-averaged Navier-Stokes techniques. Turbulent, viscous boundary-layer development plays a significant role in the development of important aerodynamic coefficients such as Magnus, drag, and roll damping. Thus, to avoid the requirement to apply multiple techniques to predict a complete set of aerodynamic performance factors, emphasis is placed on the application of the Reynolds-averaged Navier-Stokes technique.

The techniques employed have been described extensively in the literature so no detailed descriptions will be provided here. Instead, a general overview of the computational codes employed and appropriate references will be provided. The techniques employed can be categorized as time marching and space marching.

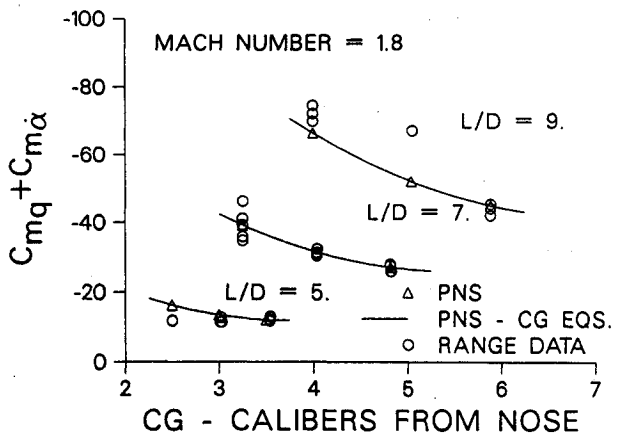

Fig. 3 Pitch-damping moment coefficient of Army-Navy spinner rocket: computation and experiment, $M=1.8$.

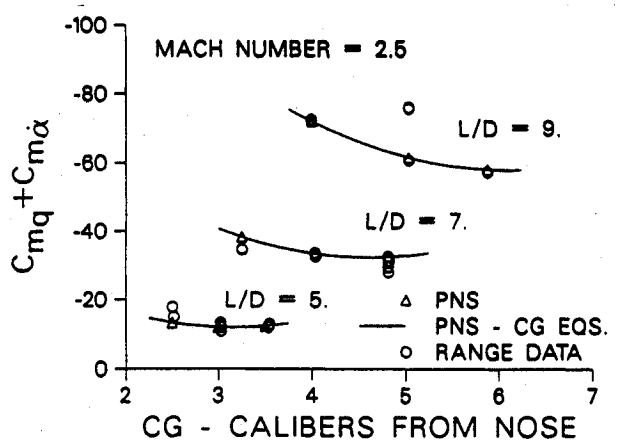

Fig. 4 Pitch-damping moment coefficient of Army-Navy spinner rocket: computation and experiment, $M=2.5$.

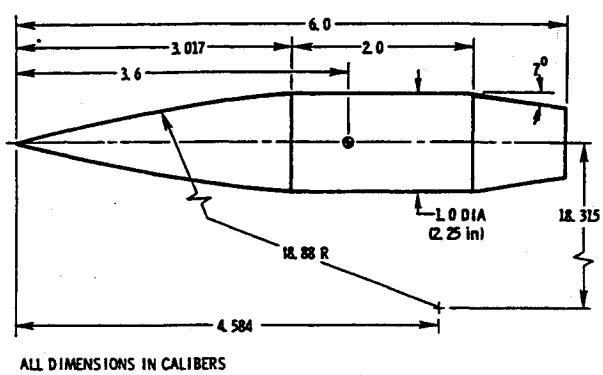

Fig. 5 Experimental SOCBT configuration.

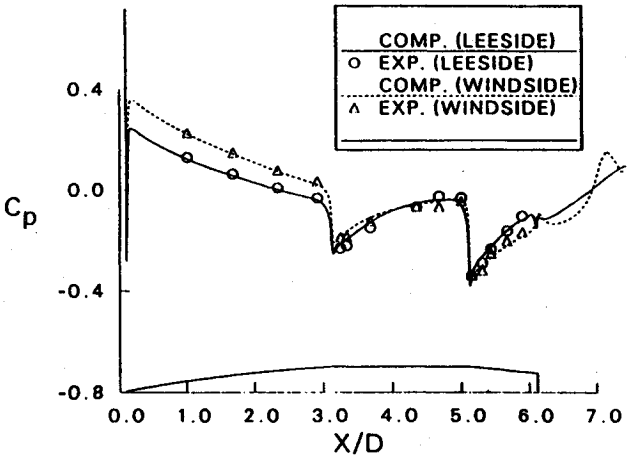

Fig. 6 Longitudinal surface pressure distribution of SOCBT projectile: $M_\infty = 1.1$ and $\alpha = 4$ deg.

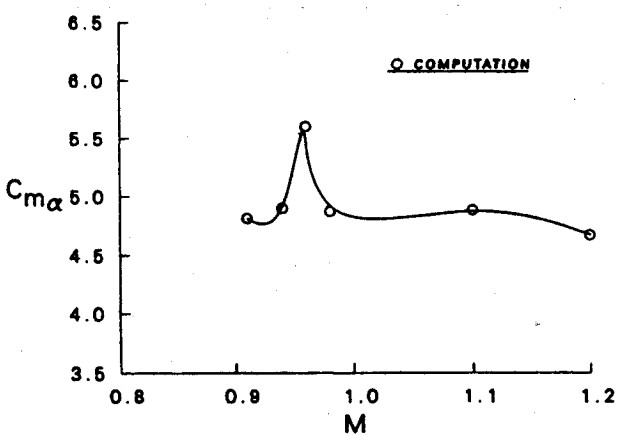

Fig. 7 Slope of pitching moment coefficient vs Mach number for SOCBT.

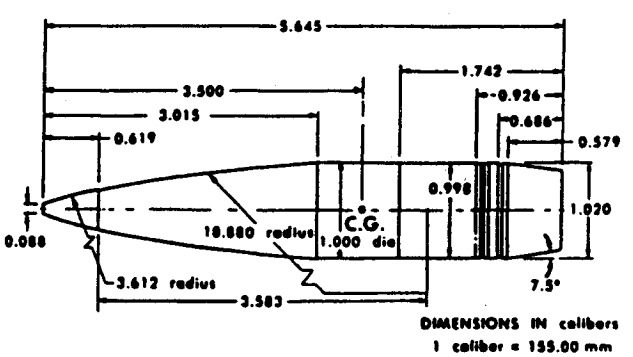

Fig. 8 M549 projectile.

The time-marching technique is used in the F3D code.[3] This technique, developed by Sahu and Steger,[3] is a flux-split, upwind scheme in the axial (main flow) direction and central differenced in the circumferential and normal direction. The F3D code provides a capability to partition the flowfield into zonal regions or blocks to accommodate complex projectiles. Since the code is time marching, it can be applied to predict subsonic and supersonic flowfields. Thus, this technique is required where regions of subsonic flow exist, such as the base region of shell, local flowfield separation, and for freestream subsonic conditions. An earlier time-marching code, which has been used to perform base flow computations including mass injection in the base region, is an extension of the azimuthal-invariant code.[4] This code is fully implicit and centrally differenced and uses the approximate factorization of Beam and Warming.[5] Projectile spin is allowed through the azimuthal-invariant assumptions.

The space-marching technique is known as the parabolized Navier-Stokes (PNS) method. The code being used was originally developed by Schiff and Steger[6] and has been extensively developed and refined by Rai and Chaussee.[7,8] This code also employs

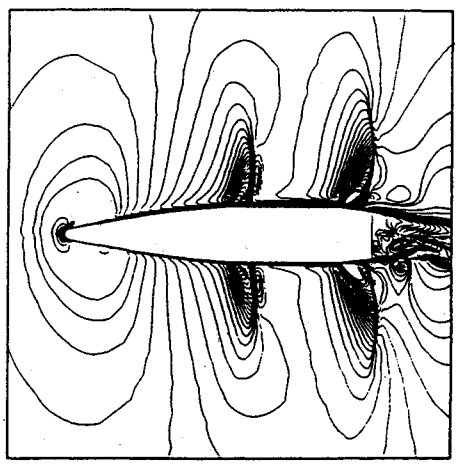

Fig. 9 Mach contours of M549 projectile: $M_\infty = 0.94$ and $\alpha = 2.0$ deg.

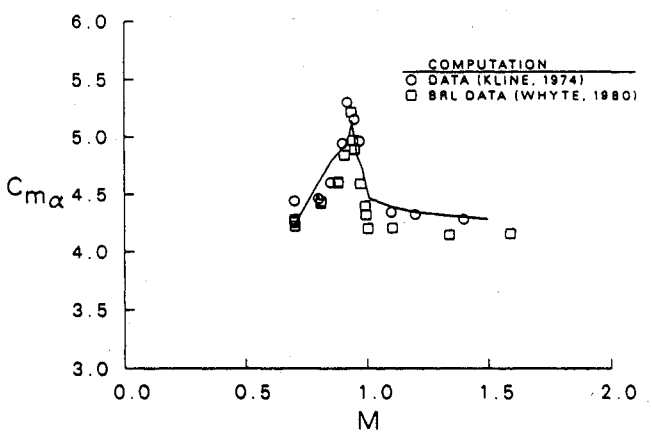

Fig. 10 Slope of pitching moment coefficient vs Mach number for M549 projectile.

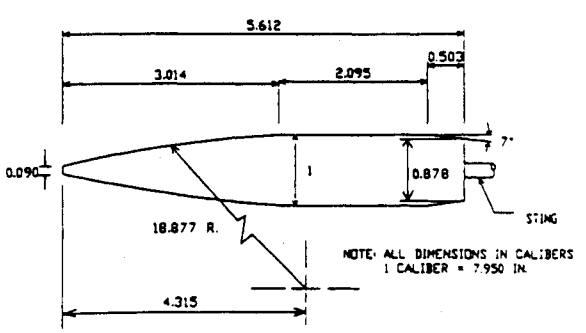

Fig. 11 Experimental wind-tunnel model with sting.

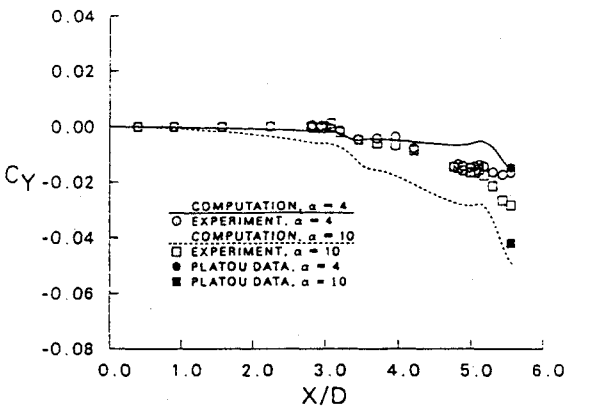

Fig. 12 Development of Magnus force along the projectile, $M_\infty = 0.94$.

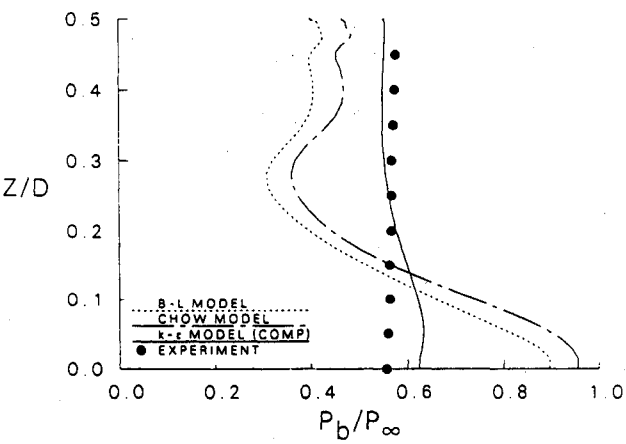

Fig. 13 Base pressure distribution: computations and experiment.

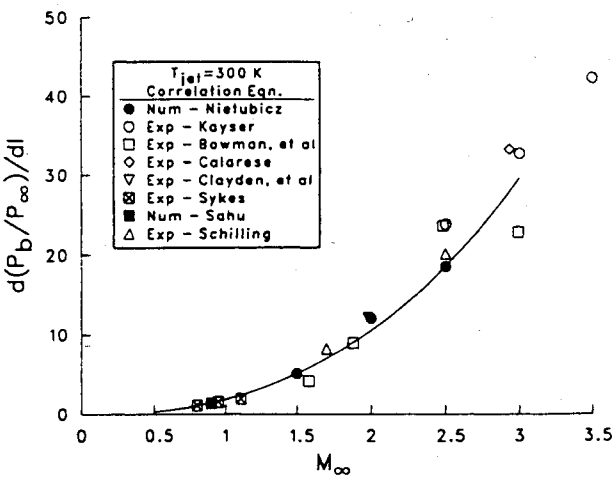

Fig. 14 $d(P_b/P_\infty)/dI$ vs M_∞: computation and experiment, $T_{oinj} = 300$ K.

the Beam-Warming linearized block, approximately factored, numerical algorithm.[5] The space-marching feature results in highly efficient use of computational resources but restricts the application to supersonic freestream conditions in which no separation in the streamwise flow occurs. This technique has proven to be highly useful in design applications for long L/D fin-stabilized projectiles that fly at high supersonic speeds and small angles of attack.

III. Grid Generation

Army projectile shapes are generally simple bodies of revolution, and a combination of elliptic, hyperbolic, and algebraic grid generator codes are used to develop the computational grids. Grid generation for the time-marching codes is carried out using either algebraic[9] or hyperbolic[10] methods. Recently, an interactive hyperbolic grid generator was developed.[11] Projectiles with irregular base region configurations and with irregular fin geometries are becoming of increasing importance. With these added complexities, the grid generation process can become lengthy and cumbersome. Grid generation for the space-marching code is carried out algebraically for the cylindrical portion of the projectile. An elliptic technique[8] is used for generating the computational grid about the fin.

IV. Turbulence Modeling

Army projectiles have surface finishes that enhance the transition to turbulence and fly under high dynamic pressure conditions at relatively low altitudes. Thus, modeling the turbulent viscous layer is important for an accurate prediction of the aerodynamic forces. The Baldwin-Lomax algebraic turbulence model[12] is routinely used for the body surface. Simple extensions of this model[13] have been found to be beneficial for computing flows in large, separated regions such as the projectile wake region and flow downstream of steps or protuberances. A more advanced k-ε model has also been applied[14] with some success. Recent results using this model have been obtained and will be discussed later.

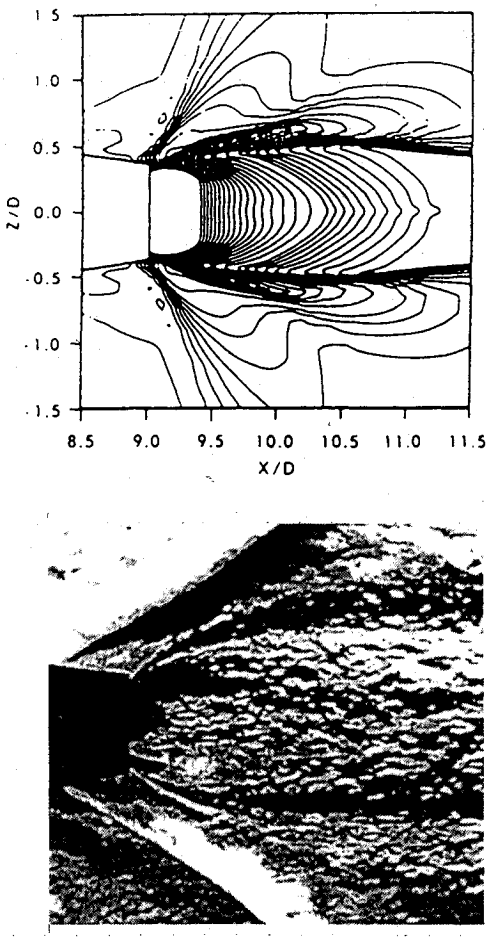

Fig. 15 Computed density contours and experimental schlieren photograph: M_∞=2.0, M_j=2.5, P_j/P_∞=9.0, jet on.

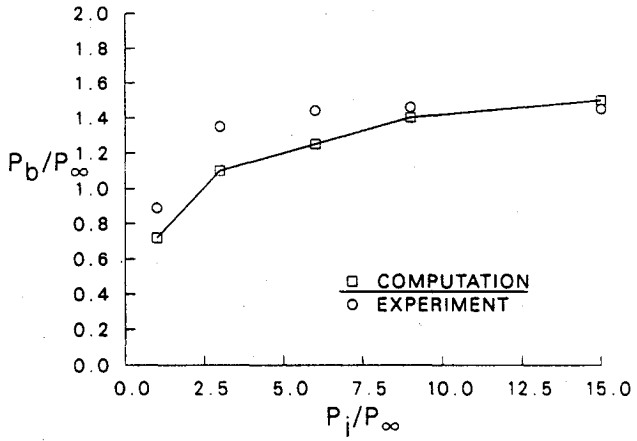

Fig. 16 Variation of base pressure with jet pressure, M_∞=2.0, jet on.

V. Validation Examples

A. Spin-Stabilized Projectiles

1. *Pitch Damping at Supersonic Velocities*

Pitch damping, according to linear theory,[15,16] is proportional to the side moment acting on a projectile undergoing a steady coning motion. This provides a convenient and efficient technique for predicting pitch damping using the PNS code in a rotating coordinate system. Thus, pitch damping can be predicted from a single computational sweep over the projectile body for a specified coning motion. Figure 1 shows a schematic illustration of the coning motion as applied here.

The prediction of pitch damping from a coning motion for bodies of revolution at supersonic velocities has been accomplished using the PNS code with modifications for centrifugal and Coriolis forces.[17] This technique has been applied to the Army-Navy spinner rocket (ANSR) configurations shown in Fig. 2. Examples of predictions for pitch damping compared with free-flight range tests for these shapes are shown in Figs. 3 and 4. These results are in excellent agreement with the data and provide solid verification of the technique. Current emphasis is being placed on extension of the technique to the time-marching numerical code, F3D. This will provide prediction capability of pitch-damping coefficients for projectiles at transonic velocities.

2. *Static and Dynamic Coefficients at Transonic Velocities*

The aerodynamics for a projectile with a boattail are known to experience a critical behavior at transonic velocities. This behavior has been shown to result from the longitudinally asymmetric shock location that occurs on the projectile at angle of attack as it traverses the transonic regime. In the previous review,[2] initial results of the computed longitudinal pressure distribution for the secant-ogive-cylinder-boattail (SOCBT) configuration shown in Fig. 5 were presented and shown to be in good agreement with the experimental data. At that time, only one Mach number had been computed using the F3D zonal code. Subsequent calculations have been performed[18] on the same configuration for a Mach number range of $0.9 \leq M \leq 1.2$ and compared with the experimental wind-tunnel data.[19] A comparison is shown in Fig. 6 between the computed wind and leeside pressure distributions and the experimental data for $M = 1.1$. The comparison is excellent and provides a sound basis for the critical behavior to be determined. The computed pitching moment coefficient shown in Fig. 7 indicates the highly localized critical behavior of a boattailed shell at transonic speeds. These results required a grid of $238 \times 39 \times 50$ points in the longitudinal, circumferential half-plane, and normal directions, respectively, to adequately resolve the shock location and thus predict the

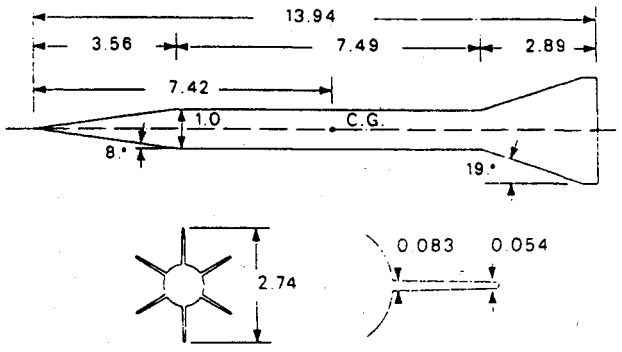

Fig. 17 Geometry of M735 projectile.

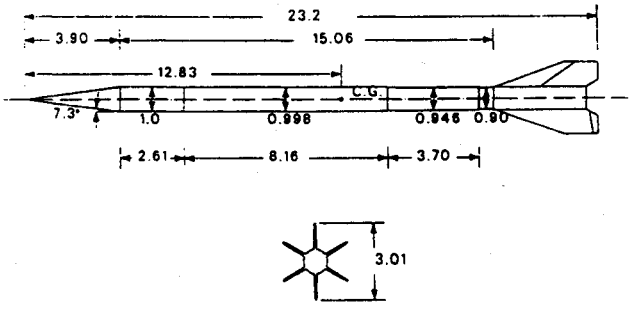

Fig. 18 Geometry of M829 projectile.

critical behavior. The run time for each Mach number on the Cray 2 was approximately 25 h.

A further test of the validation accuracy can be established by predictions of fielded Army shell. A series of computations[18] have been performed for the M549 configuration shown in Fig. 8. The Mach number ranged from $0.7 \leq M_\infty \leq 1.5$, and all computations were performed at $\alpha = 2$ deg. A representative plot of the Mach contours is shown in Fig. 9 for $M_\infty = 0.94$. The wind and leeside longitudinally asymmetric shock location is clearly evident on the boattail of the M549. The static aerodynamic coefficients have been obtained over the computed Mach number range. Figure 10 is a plot of the slope of the pitching moment coefficient comparing the computed results with the experimental data. The critical aerodynamic behavior computed is in generally good agreement with the experimental data. At most, the discrepancy is 5–7%, which is within the experimental accuracy of the flight data in the transonic regime.

A pacing item in projectile aerodynamics has been the accurate determination of the Magnus effect on a spinning projectile at transonic speeds. The Magnus effect results from a spin-induced distortion of the viscous boundary layer that exists on a spinning shell at angle of attack. Since this problem has no plane of symmetry, it is fully three dimensional and requires significant computer resources to achieve a solution. A unique experimental test was conducted by Miller and Molnar[20] in which surface pressures were measured on a spinning wind-tunnel model. The model is shown in Fig. 11. The tests were conducted for a Mach number of 0.94, at angles of attack of 0, 4, and 10 deg, and for spin rates of 0 and 4900 rpm. Computations using the F3D code were performed for this configuration at 4- and 10-deg angles of attack.[21] The grid developed for this fully three-dimensional problem consisted of three zones and required 82 million words of memory. The run time for each case on the Cray 2 was approximately 80 h. A comparison between computational and experimental data is shown in Fig. 12 for the Magnus force as it develops along the body. The pressure data has been integrated for the Magnus force and is represented by open circles and squares for 4- and 10-deg angles of attack, respectively. The solid and dashed lines are the computed results. An experimental result obtained from a wind-tunnel force balance test[22] on the same configuration is plotted as closed symbols. The results for both the 4- and 10-deg angle-of-attack cases are shown to be in good agreement with the force balance results. Although there is a discrepancy between the experimental measurements obtained using force balance and wall pressure technique as well as between the experiment and computations, the results are considered to be satisfactory given the small magnitude of the Magnus force. The computed Magnus force is in better agreement with the force balance data that is considered to be the more accurate of the two experimental results.

3. Base Flow Including Bleed and Jets

The ability to predict the base flow for shell is required for accurate determination of the projectile's total drag. The complete validation of base flow is generally quite difficult due in part to the lack of good experimental data and the uncertainty associated with applying turbulence models in the recirculating wake flow. Additional complexity is added when base bleed effects or base jets are included.

Recent tests have been conducted at the University of Illinois[23] on a cylindrical afterbody instrumented with a series of pressure taps. The model was mounted from the plenum chamber, which provided an unobstructed wake flow. Both base pressure measurements and velocity measurements of the near wake were taken for a condition of $M = 2.46$ free stream flow. The data set, which includes profiles for u and v velocities, turbulent kinetic energy, and Reynolds stress, represents a very complete set of code validation data. The F3D code, using a k-ε model and two algebraic turbulence models, was applied to the experimental configuration.[24] The upstream boundary condition was obtained from the experimental profile. Figure 13 shows the computed base pressure using the different turbulence models compared with the experimental data. Both algebraic models are shown to predict a significant variation in base pressure in the radial direction. The k-ε model results are found to be almost constant and in good agreement with the data except near the base centerline.

Validation efforts for base bleed are still not complete; however, an indication of the current predictive capability can be obtained from the results of a study for the M864 base bleed configuration. The M864 is an Army shell that burns a solid propellant in the base region. Initial computations[25] were performed using the azimuthal-invariant base flow code. The mass injection was considered to be a perfect gas at 300 K, ranging from $I = 0.005$ to 0.02. The Mach number ranged from 0.8 to 3.0. Although direct comparison with data cannot be made, a plot is shown in Fig. 14 that compares the computed results with a number of base bleed experiments.[26] The results are presented as $d(P_b/P_\infty)/dI$ vs Mach number. The computed results are in general agreement with the experimental data base.

Afterbody flows containing a propulsive jet are also of interest, and validation efforts have been under study.[2] The work described here is for an exhaust jet within an axisymmetric boattailed afterbody. The freestream Mach number is 2.0 with a jet exit of $M = 2.5$. The jet-to-freestream pressure varied from 1 to 15. The conical nozzle has a half-angle of 20 deg. Results showing the computed density contours compared with the experimental Schlieren photograph are shown in Fig. 15 for the high-pressure ratio case. Qualitative agreement can be seen in the comparison. A plot of the average base pressure as a function of exit pressure is shown in Fig. 16. The agreement is good for the pressure ratio of 9 and 15 but falls off at the lower values. Additional validation efforts are required for jet interaction problems.

B. Fin-Stabilized Projectiles

The M735 and M829 are long L/D, high-velocity, finned projectiles for which extensive aerodynamics range test data are available for comparison with computational results. These projectiles

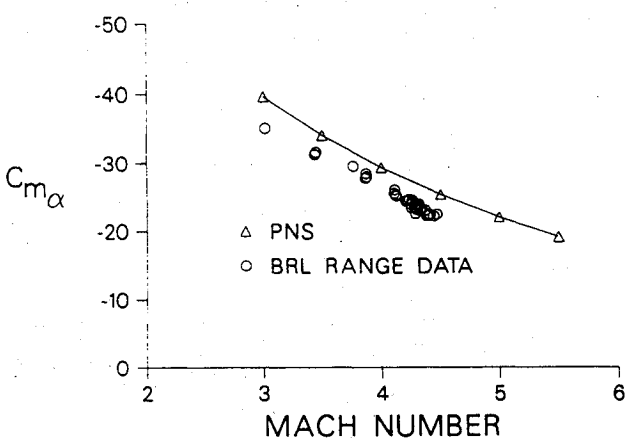

Fig. 19 Pitching moment coefficient of M735: computation and experiment.

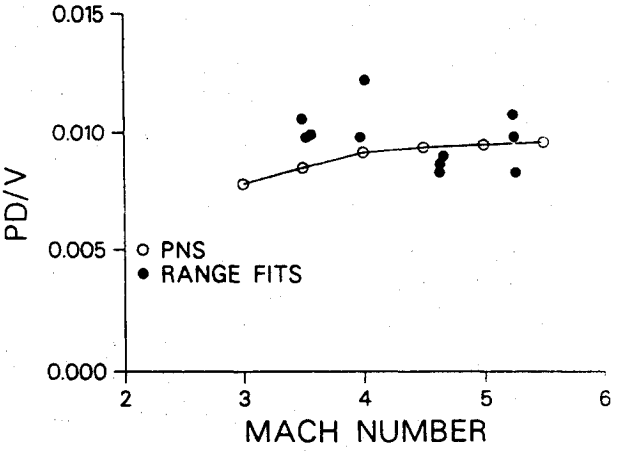

Fig. 22 Equilibrium spin rate of M829: computation and experiment.

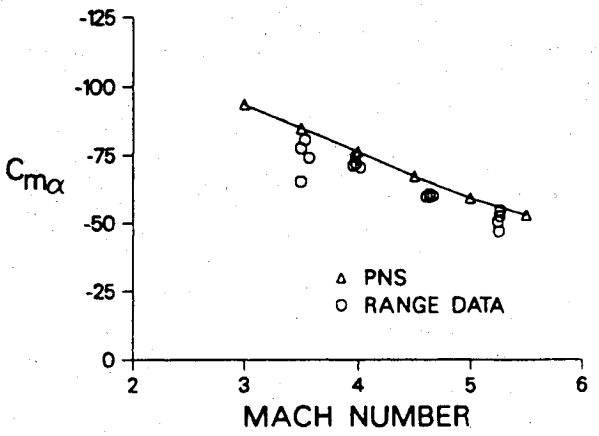

Fig. 20 Pitching moment coefficient of M829: computation and experiment.

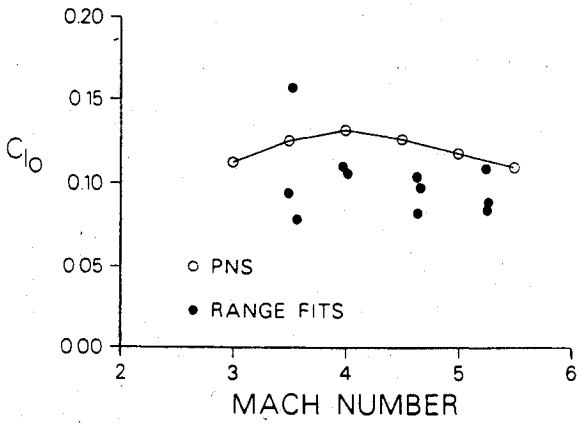

Fig. 23 Roll-producing moment coefficient of M829: computation and experiment.

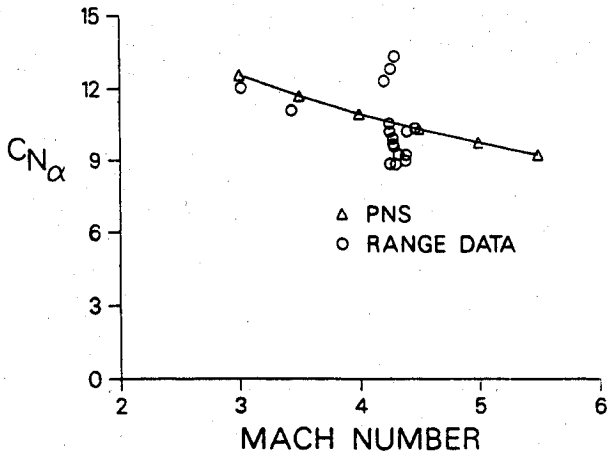

Fig. 21 Normal force coefficient of M735: computation and experiment.

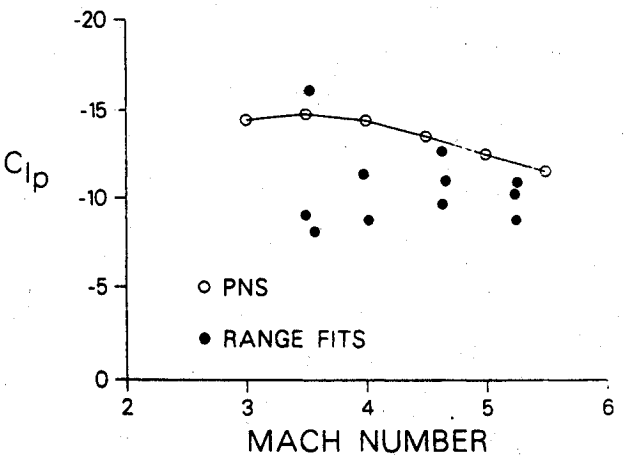

Fig. 24 Roll-damping coefficient of M829: computation and experiment.

are also of interest in that they represent a class of projectile for which developmental efforts are currently in progress. Thus, validation of computational techniques for these projectiles provides assurance to the development community that predictions for proposed projectile concepts can be carried out with confidence. The results of computational studies to predict the aerodynamics of these projectiles are reported in Refs. 27 and 28.

The geometries of the M735 and M829 are shown in Figs. 17 and 18, respectively. Computational results for the pitching moment coefficient are compared with firing data in Figs. 19 and 20 for the M735 and M829, respectively. The computed results show the same trend with Mach number as the experimental data; however, the computed results are consistently higher, by about 5%, than the experimental data. This is likely the result of neglecting the sabot grooves in the computational model. Sabot grooves cause an increase in the thickness of the boundary layer. This thickened viscous layer would be expected to decrease the effectiveness of the fins, thus reducing the magnitude of the pitching moment. The pitching moment is very accurately determined in aerodynamics range tests and is an excellent coefficient to compare

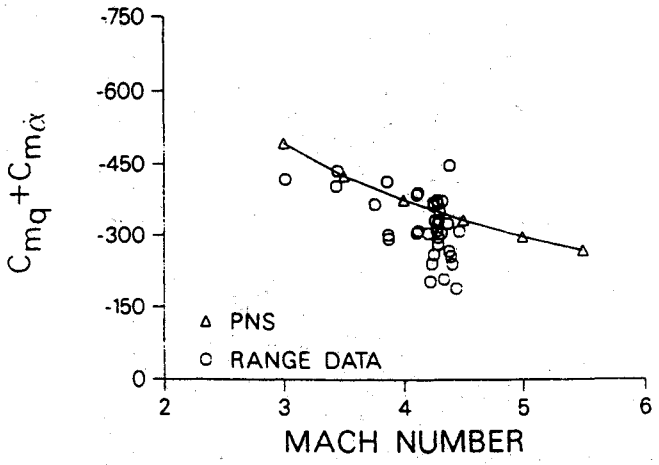

Fig. 25 Pitch-damping moment coefficient of M735: computation and experiment.

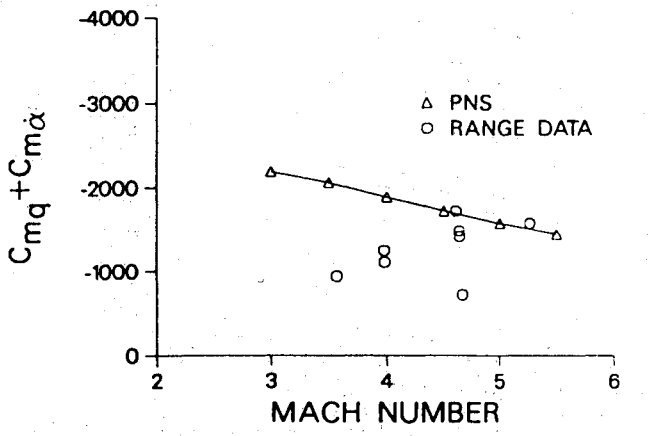

Fig. 26 Pitch-damping moment coefficient of M829: computation and experiment.

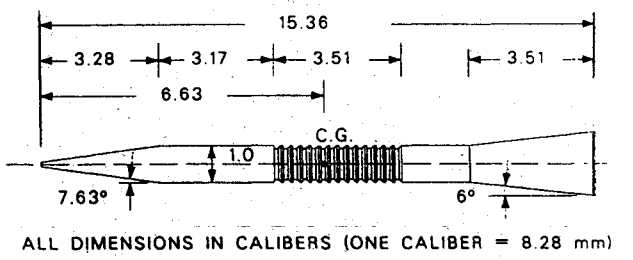

Fig. 27 Baseline flare-stabilized projectile geometry.

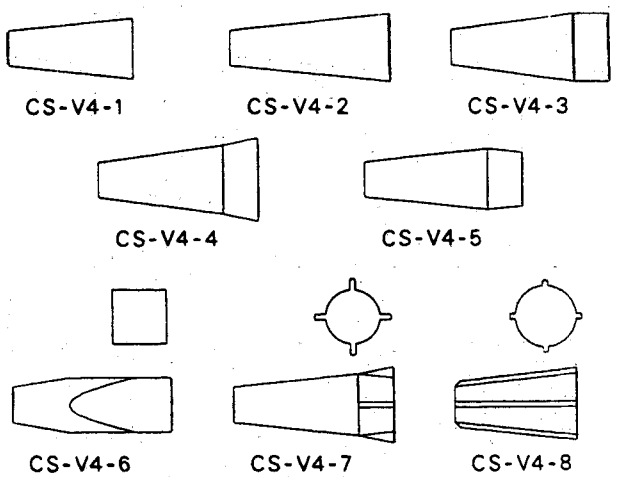

Fig. 28 Parametric flare afterbody geometries.

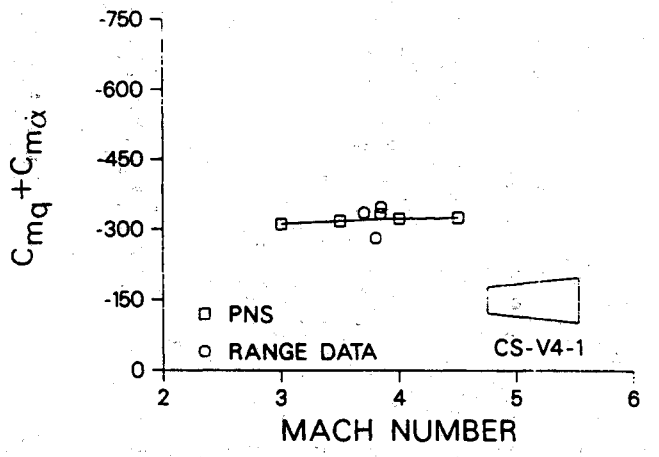

Fig. 29 Pitch-damping moment coefficient of flare V4-1: computation and experiment.

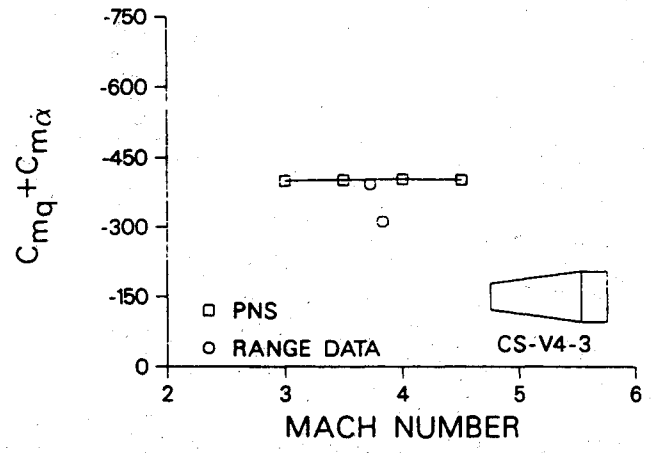

Fig. 30 Pitch-damping moment coefficient of flare V4-3: computation and experiment.

with computational results. However, the normal force is not so accurately determined experimentally due to the heavy mass of the long L/D projectiles. A comparison between computation and experiment for the normal force coefficient is shown in Fig. 21 for the M735 projectile.

Since these finned projectiles are designed to fly with a slow spin rate to reduce dispersion, dynamic coefficients such as roll damping and pitch damping are of strong interest. The projectile fins typically have leading-edge and trailing-edge cuts and chamfers to induce specific amounts of spin. The capability to predict these effects is permitted through the incorporation of the effects of centrifugal and Coriolis forces into the PNS computational code. Examples of predictions for equilibrium spin rate, roll-producing moment, and roll damping for the M829 projectile are shown in Figs. 22–24, respectively. In general, the computed results pass through the scatter in the experimental data. These particular coefficients are determined with considerable difficulty in free-flight range tests. Thus, it is of particular interest to have a predictive capability for these dynamic coefficients.

The pitch damping, as discussed previously, is proportional to the side moment acting on a projectile undergoing a steady coning motion. This provides a convenient and efficient technique for predicting the pitch damping using the PNS code in a rotating coordinate system. Thus, the pitch-damping coefficient can be predicted from a single computational sweep over the projectile body for a specified coning motion. Examples of predicted results for pitch damping are compared with experimental data for the M735 and M829 projectiles in Figs. 25 and 26, respectively. The computed results provide a consistent trend with Mach number and, in general, pass through the scatter in the experimental data. The experimental determination of pitch damping for these projectiles is

poorly determined due to the heavy mass of the projectile and the small angle-of-attack flight. To achieve better determination of the pitch damping in range tests, projectiles with the same exterior shape but with different mass distributions can be tested.

C. Flare Stabilized Projectiles

A family of flare-stabilized projectiles was studied recently through an experimental investigation in the ARL Aerodynamics Range.[29] These data have been compared with PNS computations in Refs. 30 and 31. The projectile geometries considered in this study are shown in Figs. 27 and 28.

Comparisons of pitch damping for three projectile configurations as a function of Mach number are shown in Figs. 29–31. A summary of the pitch damping results for all configurations at Mach 4 is shown in Fig. 32. These results indicate that the computational technique is capable of predicting the magnitude of the pitch damping within the experimental scatter and discriminating between the design variations.

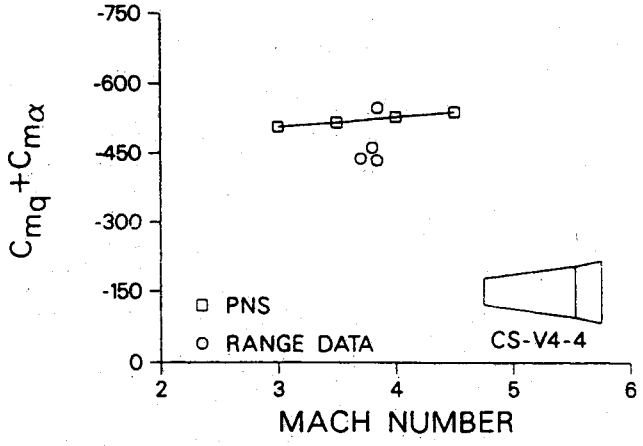

Fig. 31 Pitch-damping moment coefficient of flare V4-4: computation and experiment.

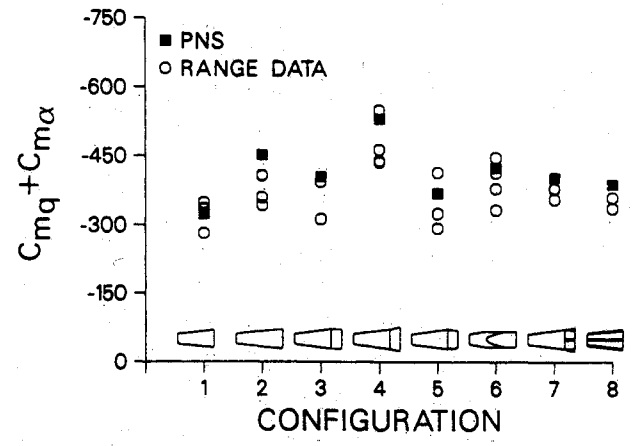

Fig. 32 Pitch-damping moment coefficient of flares at Mach 4: computation and experiment.

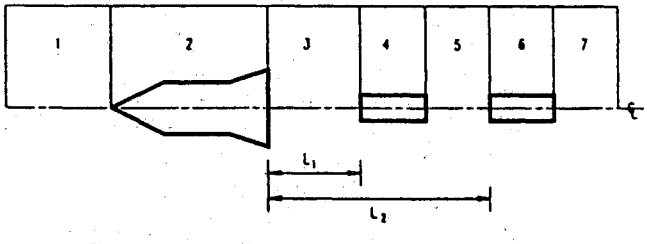

Fig. 33 Schematic diagram of multibody problem.

VI. Application Examples

The predictive capabilities have been applied recently to developmental problems in a truly predictive manner in that the computations were performed before the fabrication of hardware. The computational results provided aerodynamic flight performance information as a function of proposed design configuration and had significant influence on the configurations to be tested.

A. Scorpion Configuration

Computational support for the Scorpion project was initiated to evaluate the aerodynamic behavior of a proposed projectile concept. This concept involved a primary carrier or parent configuration with trailing cylindrical segments in the wake. A schematic of this concept is shown in Fig. 33. Aerodynamics of the lead projectile as well as a determination of the drag for the segments while in the wake of the parent projectile were of interest. Also, no known experimental or analytical data were available for this wake interaction problem.

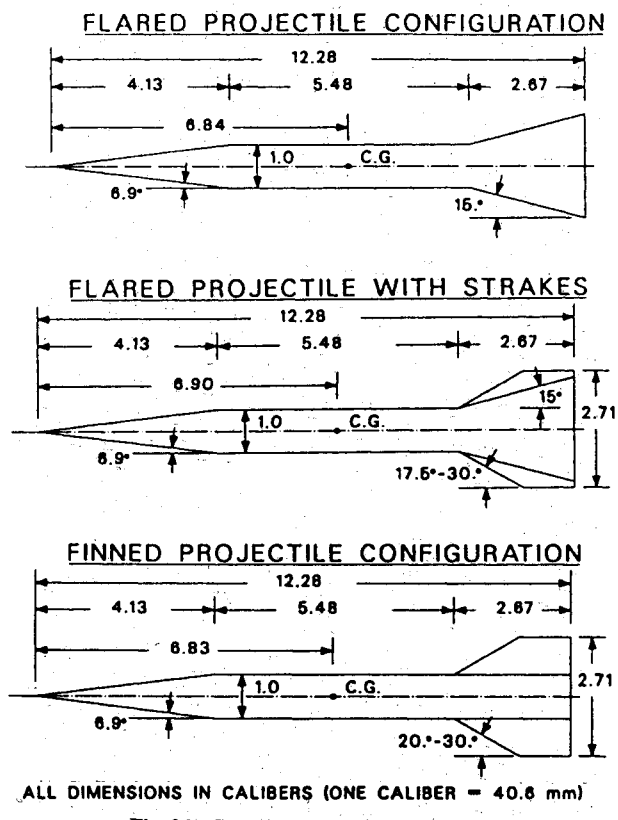

Fig. 34 Scorpion projectile configurations.

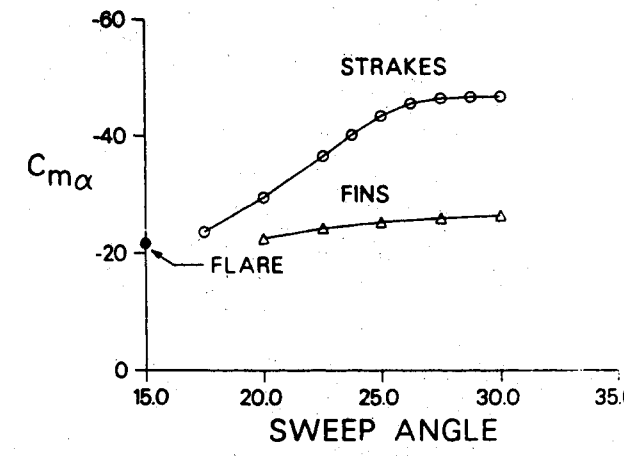

Fig. 35 Pitching moment coefficient of Scorpion configurations: computation vs sweep angle of fins and strakes.

1. *Leading Projectile Aerodynamics*

Computational aerodynamic predictions[32] were performed to determine an exterior shape to achieve optimum performance in terms of flight stability and spin rate. Three configurations for which computations have been performed are shown in Fig. 34. Computational results that compare the pitching moments and pitch damping for variations of these configurations as a function of the sweep angle for the fins and strakes are shown in Figs. 35 and 36, respectively. The pitch-damping and moments of inertia properties of the projectiles enable the pitch-damping behavior of candidate configurations to be computed. A comparison of the pitch-damping motion of the original and optimized configurations is shown in Fig. 37. The design of the straked flare was selected for the test projectile to achieve maximum damping of initial yaw and a specified spin rate at the test station. The spin rate was controlled through cant of the strakes and was determined by computations in the rotating coordinate frame. The flight tests indicated that the projectile performed in a highly satisfactory manner.

2. *Trailing Segments and Trajectory*

Multibody computations were performed[33] for the parent projectile with both one and two trailing segments at $M = 4.4$ and 0

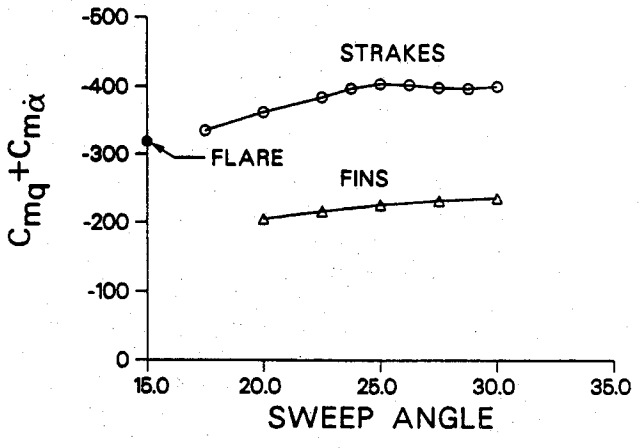

Fig. 36 Pitch-damping moment coefficient of Scorpion configurations: computation vs sweep angle of fins and strakes.

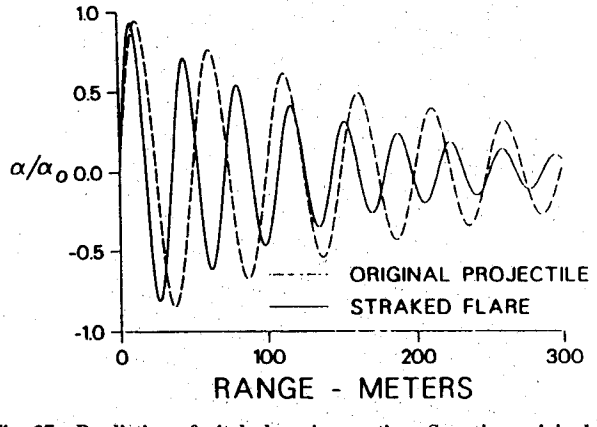

Fig. 37 Prediction of pitch-damping motion: Scorpion original and optimized configurations.

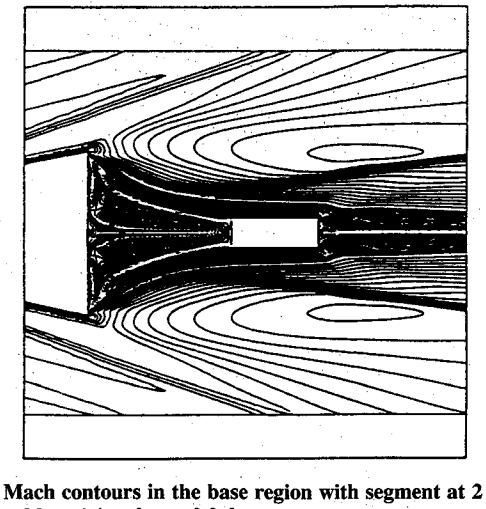

Fig. 38 Mach contours in the base region with segment at 2 calibers from base: $M_\infty = 4.4$ and $\alpha = 0.0$ deg.

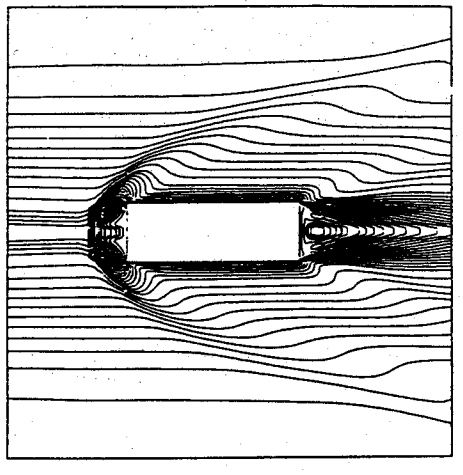

Fig. 39 Mach contours in the base region with segment at 10 calibers from base: M_∞=4.4 and α = 0.0 deg.

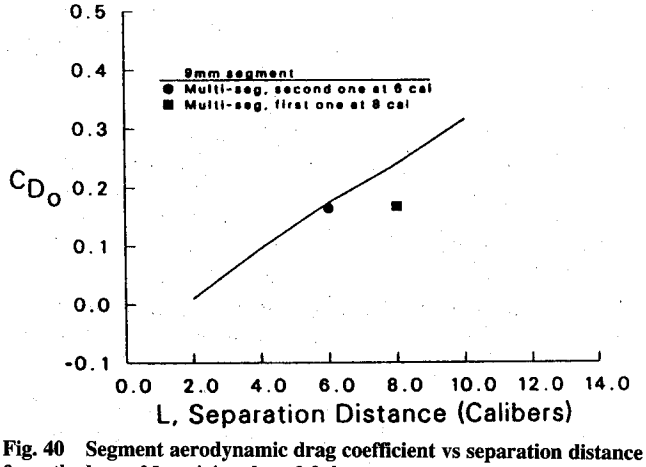

Fig. 40 Segment aerodynamic drag coefficient vs separation distance from the base: M_∞= 4.4 and α=0.0 deg.

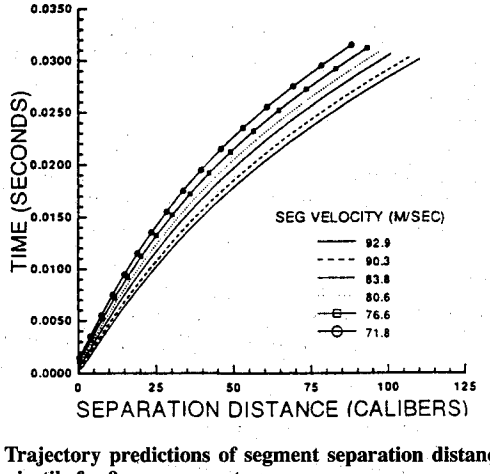

Fig. 41 Trajectory predictions of segment separation distance from parent projectile for 9-mm segment.

deg angle of attack. A series of results was obtained with the single segment configuration at various separation distances from the parent projectile. The computations were performed without considering the relative motion between parent and segment. Figure 38 shows a Mach number contour plot of the base region with the segment at 2 calibers (1 caliber is 1 parent body diameter) downstream of the base. The segment at this point is immersed within the low-speed recirculation zone of the parent projectile. When the segment is at a position of 10 calibers (Fig. 39), where the wake flow is now supersonic, a leading bow shock is seen in front of the segment. Of particular interest is the drag history for the segments, which is presented in Fig. 40. Results are shown for both one and two cylindrical segments in the wake. The drag is seen to increase as a function of separation distance for the single segment case. The multiple segment results show the decreased drag experienced by subsequent segments. The drag predictions provided valuable input to a point mass trajectory program that was used to compute the flight history for multiple segments at various initial escape velocities. The results of the trajectory computation are shown in Fig. 41. The separation distance between the base of the parent projectile and the leading segment was found to be 81 calibers (3.6 m) after the parent projectile had traveled 100 m. This computa-

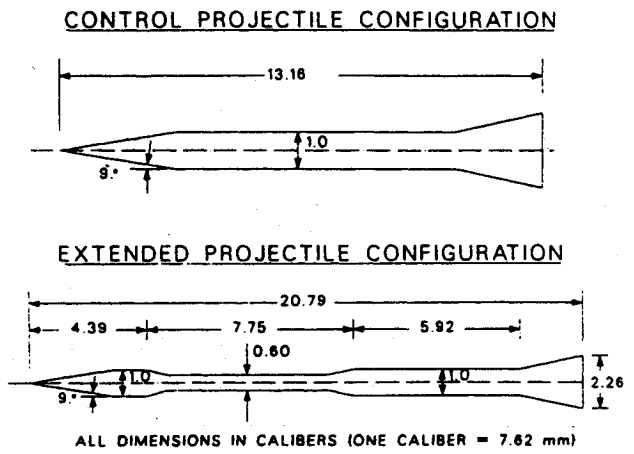

Fig. 42 Launch and extended configurations for extended rod concept.

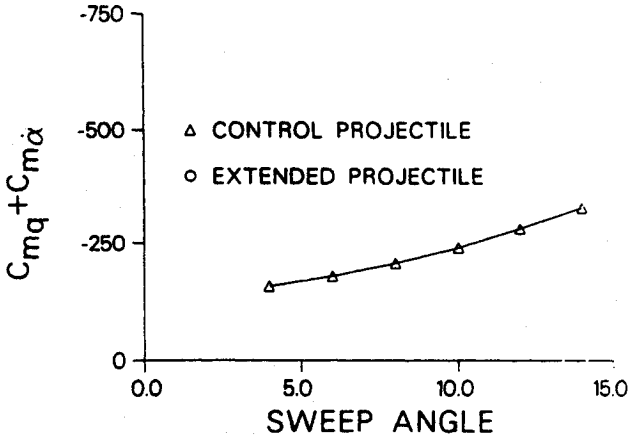

Fig. 43 Pitch-damping moment coefficient of extended rod configurations: computation vs flare sweep angle.

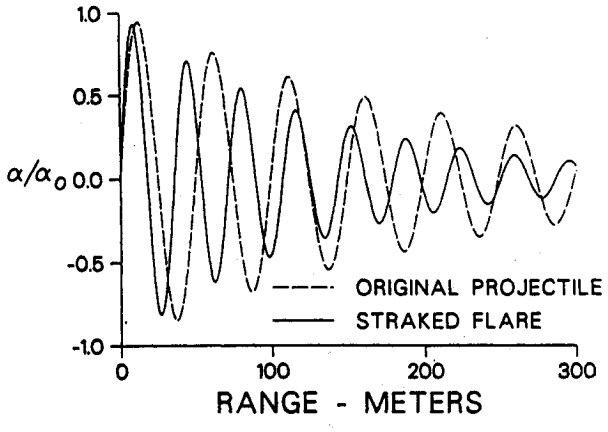

Fig. 44 Pitch-damping motion of extend rod configurations: prediction.

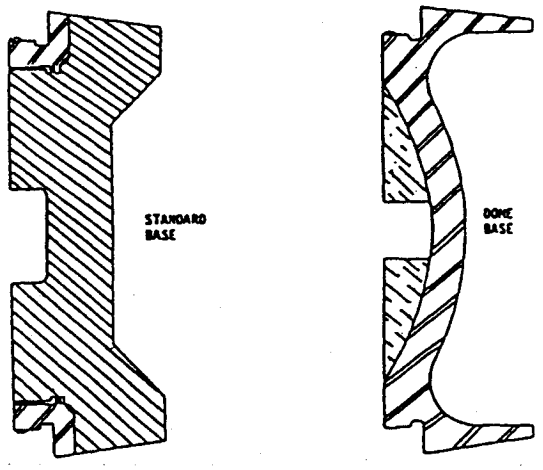

Fig. 45 Base cavity configurations.

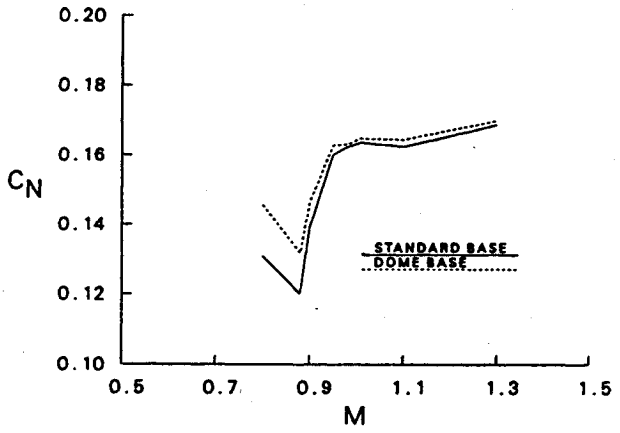

Fig. 46 Normal force coefficient vs Mach number for standard and dome base.

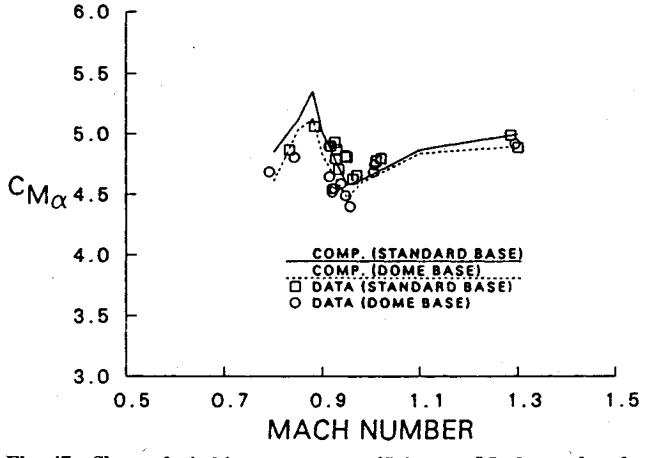

Fig. 47 Slope of pitching moment coefficient vs Mach number for standard and dome base.

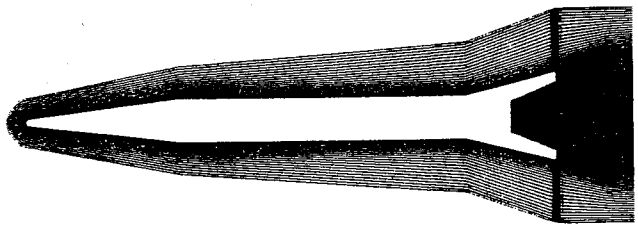

Fig. 48 Computational model of M865.

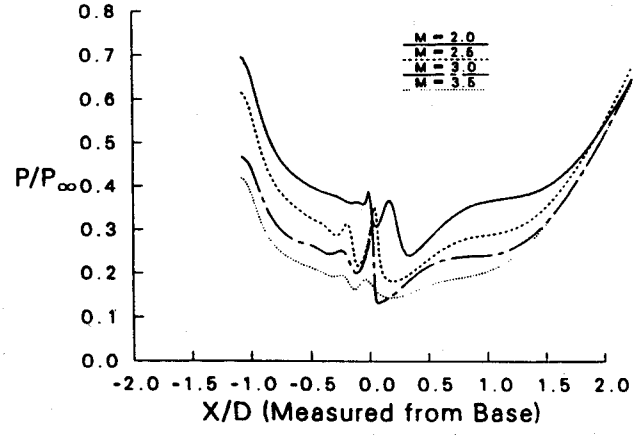

Fig. 49 Wake centerline pressure distributions: $\alpha = 0.0$ deg (original configuration).

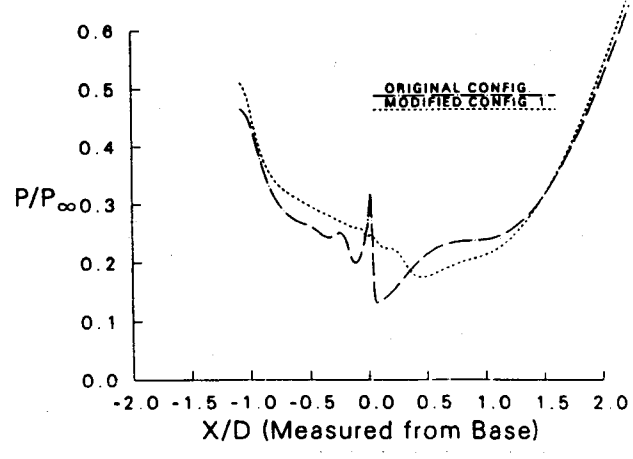

Fig. 50 Wake centerline pressure distribution: $M_\infty = 3.0$ and $\alpha = 0.0$ deg (modified configuration).

tional study was found to be useful in the design of the segments and for setting up the experimental range tests.

B. Extend Rod

The extend rod project was established to evaluate a proposed projectile concept for which the projectile extends in flight after launch. Computational aerodynamic predictions were performed to determine the flare configuration to achieve the desired drag and flight stability of the projectile in the fully extended configuration.[34] The launch and extended projectile geometries are shown in Fig. 42. The predicted pitch damping for candidate configurations as a function of flare angle is shown in Fig. 43. The predicted pitch-damping behavior is shown in Fig. 44 for the launch and extended configurations of the selected geometry. It is of interest to note that the pitch damping of the extended configuration is less rapid than the launch configuration, even though the pitch-damping moment coefficient of the extended configuration is greater. This behavior is a result of the increased longitudinal moment of inertia of the extended configuration.

C. Projectiles with Base Cavities

The majority of previous base flow computations and analytical studies considered the base of a projectile to be a flat surface. This was true even though many of the actual projectile configurations have some form of a base cavity. General opinion had been that the internal base shape was of no consequence aerodynamically and would have little or no effect on the overall flight performance parameters. Range firings of the M825 and computations for the M865, both of which have base cavities, provided evidence that the base configuration can indeed affect the base flow and, in turn, have a significant effect on the aerodynamics.

1. *M825 Projectile*

The M825 originally had an aluminum/steel base that contained a flat (standard) cavity. As a result of a product improvement initiative, a new all-steel base configuration was designed that contained a dome cavity. The base cavity configurations are shown in Fig. 45. As a result of range tests, it was found that differences in the aerodynamic performance of the two bases existed. A computational study was performed[35] to predict these differences and to further understand the fluid dynamic behavior. The computed normal force and pitching moment coefficients are shown in Figs. 46 and 47, respectively. The computations clearly show a difference in the aerodynamics between the two configurations and are in general agreement with the trend of the experimental data. An evaluation of the computed velocity vectors indicated that the changes were due in part to a displacement of the shear layer near the base corner of the standard configuration, which weakened the expansion at the base corner.

2. *M865 Projectile*

The M865 is a flare-stabilized projectile that simulates the flight of long L/D-finned projectiles for training purposes. The M865 contains a tracer in the base cavity. In firing tests, it was noticed that the tracer, which the gunner uses to detect the impact point of the round, was not visible for the full range of interest. In an effort

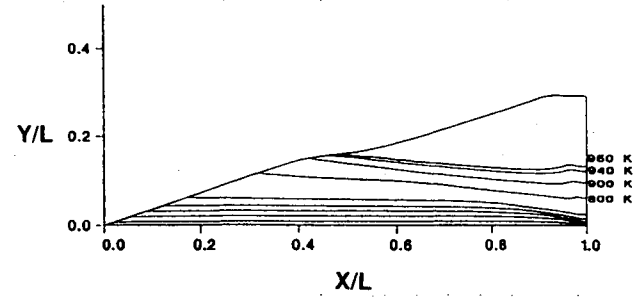

Fig. 51 Temperature contours of M829 with aluminum oxide coating, flight time = 2.0 s.

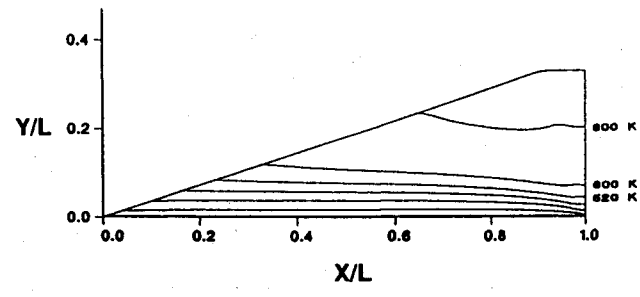

Fig. 52 Temperature contours of M829 with fiber/epoxy coating, flight time = 2.0 s.

to uncover a cause for this unsatisfactory performance, a computational study was carried out in which the pressure distribution in the wake of the projectile was computed. The computational study[36] was conducted for the velocity range of interest, $2.0 \leq M \leq 5.0$. Figure 48 shows the computational model of the M865, including the base region cavity. The computations did not consider any mass injection effects. An analysis of the base flow results indicated the presence of a pressure spike located along the axis near the base of the projectile. Figure 49 is a plot of the centerline pressure extending from the interior cavity downstream. The jump in pressure can be seen for all Mach numbers with the largest spike occurring at $M = 3.0$. This rapid pressure change was considered as a potential reason for the premature tracer burnout. In an attempt to reduce or eliminate this problem, a modified cavity design was proposed and computations were performed. The results, shown in Fig. 50, are again in the form of centerline pressure for the $M = 3.0$ case. The comparison between the original and modified configurations shows that the original pressure spike has been reduced. This result has provided a potential cause for the unexpected behavior of the M865 projectile.

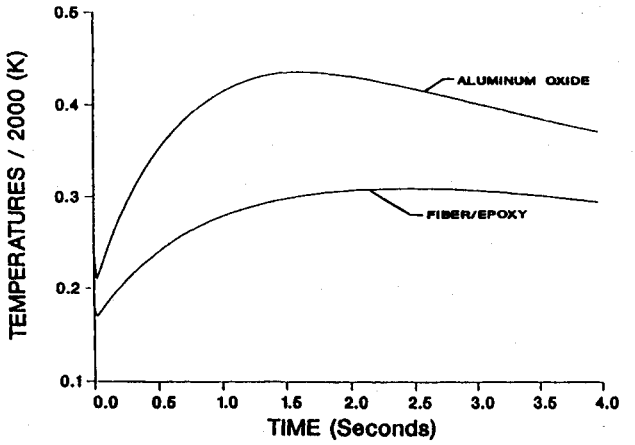

Fig. 53 Temperature at M829 fin leading edge vs flight time, aluminum oxide and fiber/epoxy coatings.

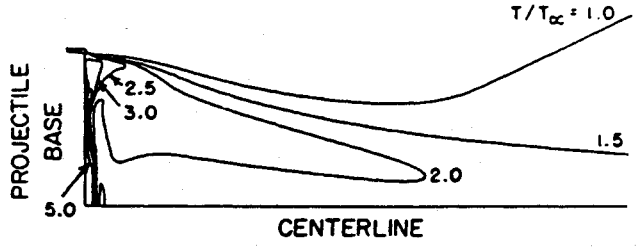

Fig. 54 Temperature contours: hot air injection, $M_\infty = 2$, $I = 0.0022$, $T_\infty = 294$ K, $T_w = 294$, and $T_{oinj} = 1533$ K.

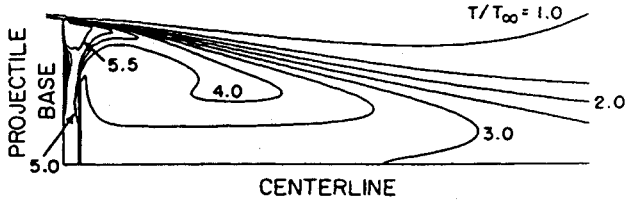

Fig. 55 Temperature contours: H_2-CO injection, $M_\infty = 2$, $I = 0.0022$, $T_\infty = 294$ K, $Tw = 294$, and $T_{oinj} = 1533$ K.

VII. Aerodynamic Heating

The stabilizing fins for long L/D kinetic energy (KE) penetrator projectiles are made of aluminum alloy. Since the melting temperature of aluminum is approximately 960 K, these fins are vulnerable to the effects of in-bore and aerodynamic heating. No direct experimental measurements of the heating rates or temperature response of these fins are available due to the difficult environment and thin geometry of the fins. However, qualitative visual and photographic observations during flight tests, which reveal structural deficiencies such as altered planform shape and "burning" of the fins, are available to indicate that melt temperature is reached for these fins.

Several studies to model the in-bore and free flight aerodynamic heating for these fins have been performed.[37–39] A recent study[39] reports results in which a newly developed finite volume heat conduction code[38] was used to predict the benefit of protective coating materials for fins. The computations included the effect of retardation of the projectile in flight through time-dependent boundary conditions for convective heat transfer and recovery temperature based on the known flight trajectory. The convective heat transfer and recovery temperature boundary conditions were determined using PNS code results for the full projectile with fins. Examples of the results achieved are shown in Figs. 51–53. Temperature contours for a flight time of 2.0 s for the aluminum fin with standard aluminum oxide coating is shown in Fig. 51 and for the same conditions with a fiber epoxy coating in Fig. 52. The temperature at the leading edge of the fin at midspan is shown in Fig. 53 as a function of flight time for the two coating materials. The substantial benefit of the ablative coating is illustrated.

The effects of aerodynamic heating are becoming increasingly important as the Army considers the development of longer range artillery shell and increased launch velocities using electromagnetic and electrothermal launcher technologies.

VIII. Research Areas

Although a highly sophisticated computational predictive capability for projectile aerodynamics currently exists, active research is being carried out to further develop and refine this predictive capability. In particular, techniques for combustion modeling, zonal modeling techniques, and optimization of numerical algorithms for efficient utilization of massively parallel computer architectures are of interest. Requirements for improved turbulence modeling are expected to become of critical importance in the near future in applications where significant regions of flow separation occur such as high angles of attack and for highly deflected guidance fins.

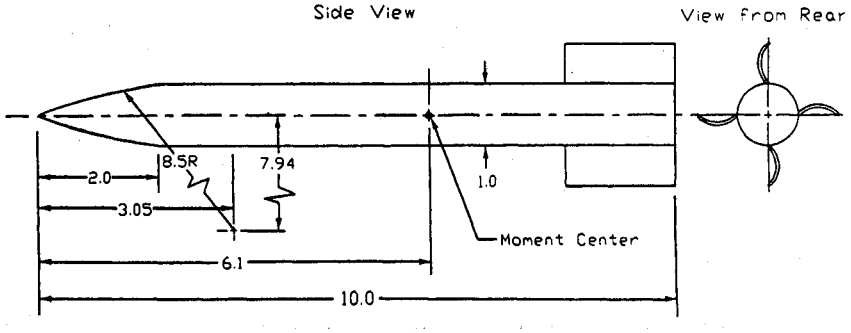

Fig. 56 Wraparound fin projectile geometry.

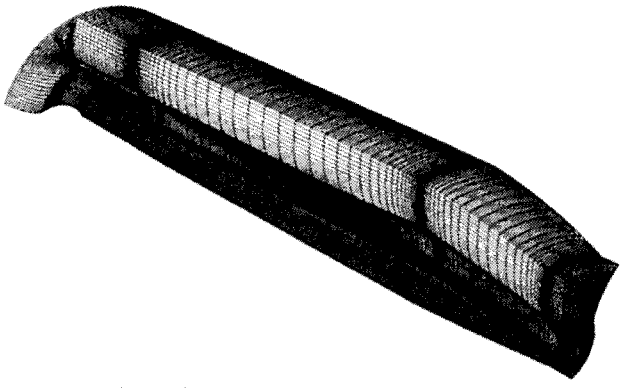

Fig. 57 Wraparound fin projectile grid.

A. Combustion Modeling

Combustion modeling is of interest to predict the effects of the burning of solid propellants for base-bleed and rocket-assist projectiles. These concepts are used to achieve increased range for artillery projectiles, which is an area of current interest.

An initial attempt to obtain a combustion capability for base-bleed projectiles was begun through a contract with Scientific Research Associates. The computational approach that has been used for this effort was developed by Giebling and Buggeln.[40] Several combustion models that would be applicable to the projectile base flow problem were evaluated. The code (CMINT) is based on the solution of the Navier-Stokes equations coupled with the species conservation and turbulence model equations. Injectant gas mixtures of H_2 and H_2/CO were considered and applied to a flat base projectile configuration. Computations were performed on a flat base M864 configuration for conditions without bleed, with hot air bleed, and with reacting H_2/CO injection. All computations were performed at $M = 2.0$ and 0 deg angle of attack. A combustion model consisting of 9 species and 12 reactions was used. Temperature contours are shown in Figs. 54 and 55 for hot mass injection and combustion, respectively. The effect of the hot mass injection is seen to be confined very near the base, whereas combustion affects the entire recirculation region. The net decrease in base drag when combustion is added was found to be approximately 20%.

B. Zonal Techniques

Techniques to subdivide the projectile flowfield into zones for ease and convenience of grid generation for highly complex projectile configurations are being pursued. Improved techniques for specifying the zonal boundaries and boundary conditions are needed to reduce the time required to generate computational grids and to set up the flowfield solver. Guided projectile configurations with deflected fins and gaps between the fin and projectile body represent a significant challenge. The wraparound fin projectile, Fig. 56, is another example of a configuration that could benefit from improved zonal techniques. An example of a grid generated for a wraparound configuration[41] is shown in Fig. 57. The time required to set up this geometry for solution by a Navier-Stokes code exceeded three months. Clearly, there is room for improvement in the structure of the Navier-Stokes solver and the grid generation technique.

In an attempt to provide more efficient methods for complex projectile configurations, research is currently being conducted to apply overset or Chimera[42] technology to multibody problems with relative motion. An example of a multibody problem is the Scorpion project described earlier. This work is in its initial stage and involves using the F3D code combined with a domain decomposition code called DCL3D developed by Meakin and Suhs.[43] The computational approach is completed by applying the computed aerodynamic loads to the multiple bodies and computing the trajectory. This determines the position of the moving bodies for the next time step of the flow solver. This approach has been applied[44] with success to the Space Shuttle store separation process.

C. Turbulence Modeling

The Baldwin-Lomax algebraic turbulence model and simple modifications of this model have been used with good success for many Army projectile applications. However, as the configurations become more complex and the angles of attack considered result in flow with significant regions of flow separation, more advanced turbulence models will be required. Current efforts include the application of k-ε modeling in the base region of shell. The proper wake turbulence model for flows with combustion taking place is currently unknown. Another challenging application is the prediction of flow in the wake of finned projectiles. The relatively thin, blunt trailing edges of these fins require modeling techniques to resolve the free shear layers downstream of the fins and in the wake region of the projectile base.

D. Massively Parallel Techniques

The solutions of complex projectile applications such as guided configurations, projectiles with combustion taking place in the base region, and transonic flight at large angles of attack require computers with greater than 100 million words of memory and result in computation times of greater than 50 h on a Cray 2 class CPU. For CFD to provide timely input to the projectile design process, several orders of magnitude increases in computer memory and processing speed are required. This will only be achieved through successful optimization of computational techniques for massively parallel computer architectures. Efforts to achieve this enhanced capability are of great interest.

IX. Concluding Remarks

The applied computational projectile aerodynamic research described herein represents a summary of recent experience at the U.S. Army Research Laboratory. It is believed that a highly productive capability currently exists to help projectile designers achieve optimized aerodynamic configurations. This is particularly true for supersonic velocity flight for spin-, fin-, and flare-stabilized projectiles. The predictive capabilities described have been applied to a wide variety of recent projectile development projects with considerable success.

Areas in which further development of the predictive technology is desirable have been outlined. Research is ongoing at the U.S. Army Research Laboratory to address these deficiencies; however, relevant research efforts in other government research institutions and academia are encouraged.

Acknowledgments

The results presented represent the efforts of several engineers and support personnel in the Aerodynamics Branch of the Propulsion and Flight Division of the U.S. Army Research Laboratory. In particular, the efforts of J. E. Danberg, H. L. Edge, B. J. Guidos Jr., K. R. Heavey, R. A. Larkin, and J. V. Smith deserve special recognition.

References

[1]Sturek, W. B., "Application of CFD to the Aerodynamics of Spinning Shell," AIAA Paper 84-0323, Jan. 1984.

[2]Nietubicz, C. J., and Sturek, W. B., "Navier-Stokes Code Verification for Projectile Configurations at Supersonic and Transonic Velocities," AIAA Paper 88-1995, May 1988.

[3]Sahu, J., and Steger, J. L., "Numerical Simulation of Three Dimensional Transonic Flows," U.S. Army Ballistic Research Lab., BRL-TR-2903, Aberdeen Proving Ground, MD, March 1988 (also AIAA Paper 87-2293, 1987).

[4]Nietubicz, C. J., Pulliam, T. H., and Steger, J. L., "Numerical Solution of the Azimuthal-Invariant Thin-Layer Navier-Stokes Equations," *AIAA Journal*, Vol. 18, No. 12, 1980, pp. 1411, 1412.

[5]Beam, R., and Warming, R. F., "An Implicit Factored Scheme for the Compressible Navier-Stokes Equations," *AIAA Journal*, Vol. 16, No. 4, 1978, pp. 393–402.

[6]Schiff, L. B., and Steger, J. L., "Numerical Simulation of Steady Supersonic Viscous Flow," *AIAA Journal*, Vol. 18, No. 12, 1980, pp. 1421–1430.

[7]Rai, M. M., and Chaussee, D. S., "New Implicit Boundary Procedure: Theory and Applications," AIAA Paper 83-0123, Jan. 1983.

[8]Rai, M. M., Chaussee, D. S., and Rizk, Y. M., "Calculation of Viscous

Supersonic Flows over Finned Bodies," AIAA Paper 83-1667, July 1983.

[9]Steger, J. L., Nietubicz, C. J., and Heavey, K. R., "A General Curvilinear Grid Generation Program for Projectile Configurations," U.S. Army Ballistic Research Lab., BRL-MR-03142, Aberdeen Proving Ground, MD, Oct. 1981.

[10]Nietubicz, C. J., Heavey, K. R., and Steger, J. L., "Grid Generation Techniques for Projectile Configurations," *Proceedings of the 1982 Army Numerical Analysis and Computers Conference,* ARO Rept. 82-3, Oct. 1982, pp. 99–121.

[11]Ferry, E. N., Jr., and Nietubicz, C. J., "Interactive Hyperbolic Grid Generation for Projectile CFD," U.S. Army Ballistic Research Lab., BRL-MR-3971, Aberdeen Proving Ground, MD, May 1992.

[12]Baldwin, B. S., and Lomax, H., "Thin Layer Approximation and Algebraic Model for Separated Turbulent Flows," AIAA Paper 78-257, Jan. 1978.

[13]Chow, W. L., "Improvement on Numerical Computation of the Thin-Layer Navier-Stokes Equation—with Emphasis on the Turbulent Base Pressure of a Projectile in Transonic Flight Condition," Univ. of Illinois Contract Rept., Contract DAAG29-81-D-0100, Urbana, IL, Nov. 1985.

[14]Sahu, J., and Danberg, J. E., "Navier-Stokes Computations of Transonic Flow with a Two Equation Model," *AIAA Journal,* Vol. 24, No. 11, 1986, pp. 1744–1751.

[15]Murphy, C. H., "Free Flight Motion of Symmetric Missiles," U.S. Army Ballistic Research Lab., BRL Rept. 1216, Aberdeen Proving Ground, MD, July 1963.

[16]Tobak, M., Schiff, L. B., and Peterson, V. L., "Aerodynamics of Bodies of Revolution in Coning Motion," *AIAA Journal,* Vol. 7, No. 1, 1969, pp. 95–99.

[17]Weinacht, P., Sturek, W. B., and Schiff, L. B., "Navier-Stokes Predictions of Pitch Damping for Axisymmetric Shell Using Steady Coning Motion," AIAA Paper 91-2855, Aug. 1991.

[18]Sahu, J., "Transonic Critical Aerodynamic Behavior," *AIAA Journal,* Vol. 28, No. 5, 1990, pp. 807–816 (also U.S. Army Ballistic Research Lab., BRL-TR-2962, Aberdeen Proving Ground, MD, Dec. 1988).

[19]Kayser L. D., and Whiton, F., "Surface Pressure Measurements on a Boattailed Projectile Shape at Transonic Speeds," U.S. Army Ballistic Research Lab., BRL-MR-03161, Aberdeen Proving Ground, MD, March 1982.

[20]Miller, M. C., and Molnar, J. W., "Wind Tunnel Measurements of the Magnus Induced Surface Pressures on a Spinning Artillery Projectile Model in the Transonic Speed Regime," Chemical Research, Development and Engineering Center, CRDEC-TR-86081, Aberdeen Proving Ground, MD, Sept. 1986.

[21]Sahu, J., "Transonic Navier-Stokes Computations for a Spinning Body of Revolution," U.S. Army Ballistic Research Lab., BRL-TR-3265, Aberdeen Proving Ground, MD, Sept. 1991.

[22]Platou, A. S., and Nielsen, G. I. T., "Some Aerodynamic Characteristics of the Artillery Projectile XM549," U.S. Army Ballistic Research Lab., BRL-MR-2284, Aberdeen Proving Ground, MD, April 1973.

[23]Herrin, J. L., and Dutton, J. C., "An Experimental Investigation of the Supersonic Axisymmetric Base Flow Behind a Cylindrical Afterbody," Univ. of Illinois at Urbana-Champaign, UICU 91-4004, Urbana, IL, May 1991.

[24]Sahu, J., "Numerical Computations of Supersonic Base Flow with Special Emphasis on Turbulence Modeling," AIAA Paper 92-4352, Aug. 1992.

[25]Nietubicz, C. J., and Sahu, J., "Navier-Stokes Computations of Base Bleed Projectiles," *Base Bleed: First International Symposium on Special Topics in Chemical Propulsion,* edited by K. K. Kuo and J. F. Fleming, Hemisphere, Washington, DC, 1991, pp. 93–106.

[26]Danberg, J. E., and Nietubicz, C. J., "Predicted Flight Performance of Base-Bleed Projectiles," *Journal of Spacecraft and Rockets,* Vol. 29, No. 3, 1992, pp. 366-372.

[27]Weinacht, P., and Sturek, W. B., "Navier-Stokes Predictions of Static and Dynamic Aerodynamic Derivatives for High L/D Projectiles," *Proceedings of the 66th AGARD Fluid Dynamics Panel Symposium on Missile Aerodynamics,* Friedrichshafen, Germany, April 1990.

[28]Weinacht, P., and Sturek, W. B., "Navier-Stokes Predictions of Pitch Damping for Finned Projectiles Using Steady Coning Motion," AIAA Paper 90-3088, Aug. 1990.

[29]Celmins, I., "Aerodynamic Characteristics of Fin and Flare-Stabilized 25mm XM910 Prototypes," U.S. Army Ballistic Research Lab., BRL-TR-2882, Aberdeen Proving Ground, MD, Dec. 1987.

[30]Weinacht, P., "Navier-Stokes Prediction of Pitch Damping for a Family of Flared Projectiles," AIAA Paper 91-3339, Sept. 1991.

[31]Danberg, J. E., Sigal, A., and Celmins, I., "Aerodynamic Characteristics of a Family of Cone-Cylinder-Flare Projectiles," *Journal of Spacecraft and Rockets,* Vol. 27, No. 4, 1990, pp. 355-360.

[32]Weinacht, P., "Aerodynamic Predictions for the Scorpion Parent Projectile Using a Navier-Stokes Approach," U.S. Army Ballistic Research Lab., BRL-TR-3350, Aberdeen Proving Ground, MD, June 1992.

[33]Sahu, J., and Nietubicz, C. J., "A Computational Study of Cylindrical Segments in the Wake of a Projectile," U.S. Army Ballistic Research Lab., BRL-TR-3254, Aberdeen Proving Ground, MD, Aug. 1991.

[34]Weinacht, P., "Aerodynamic Predictions for Extending Projectile Designs," U.S. Army Ballistic Research Lab., BRL-TR-3350, Aberdeen Proving Ground, MD, June 1992.

[35]Sahu, J., and Nietubicz, C. J., "Three Dimensional Flow Calculations for a Projectile with Standard and Dome Bases," Society of Automotive Engineers, SAE Paper 89-2291, Warrendale, PA, Sept. 1989.

[36]Sahu, J., "A Computational Study of the Base Region Flow Field for the M865 Projectile," U.S. Army Research Lab., ARL-TR-109, Aberdeen Proving Ground, MD.

[37]Sturek, W. B., Kayser, L. D., and Weinacht, P., "Computational Study of Swept-Fin Aerodynamic Heating for the 105mm M774," U.S. Army Ballistic Research Lab., ARBRL-MR-03315, Aberdeen Proving Ground, MD, Oct. 1983.

[38]Sturek, W. B., Dwyer, H. A., and Ferry, E. N., Jr., "Prediction of In-Bore and Aerodynamic Heating of KE Projectile Fins," U.S. Army Ballistic Research Lab., BRL-MR-3852, Aberdeen Proving Ground, MD, Aug. 1990.

[39]Sturek, F. D., Sturek, W. B., and Ferry, E. N., Jr., "A Computational Study of the Effectiveness of Coating Materials for KE Projectile Fins Subjected to the Combined Effects of Inbore and Aerodynamic Heating," U.S. Army Ballistic Research Lab., BRL-MR-3831, Aberdeen Proving Ground, MD, April 1990.

[40]Giebling, H. J., and Buggeln, R. C., "Reacting Flow Models for Navier-Stokes Analysis of Projectile Base Combustion," AIAA Paper 91-2077, June 1991.

[41]Edge, H. L., "Computation of the Roll Moment Coefficient for a Projectile with Wrap-Around Fins," U.S. Army Research Lab., ARL-TR-23, Aberdeen Proving Ground, MD, Dec. 1992.

[42]Benek, J. A., Buning, P. G., and Steger, J. L., "A 3-D Chimera Grid Embedding Technique," AIAA Paper 85-1523, July 1985.

[43]Meakin, R. L., and Suhs, N., "Unsteady Aerodynamic Simulation of Multiple Bodies in Relative Motion," AIAA Paper 89-1996, June 1989.

[44]Meakin, R. L., "Overset Grid Methods for Aerodynamic Simulation of Bodies in Relative Motion," *8th Aircraft/Stores Compatibility Symposium,* Ft. Walton Beach, FL, Oct. 1990.